Annual Review of Chaos Theory, Bifurcations and Dynamical Systems
Vol. 7, (2017) 41-55, www.arctbds.com.

Effect of Narrow Band Frequency Modulated Signal on Horseshoe Chaos in Nonlinearly Damped Duffing-vander Pol Oscillator

M.V. Sethumeenakshi
Department of Mathematics, St.Xavier's College, Palayamkottai-627 002, Tamilnadu, India.
e-mail: sethumeenakshi91@gmail.com

S. Athisayanathan
Department of Mathematics, St.Xavier's College, Palayamkottai-627 002, Tamilnadu, India.
e-mail: athisayanathan@yahoo.co.in

V. Chinnathambi
Department of Physics, Sri K.G.S. Arts College, Srivaikuntam-628 619, Tamilnadu, India.
e-mail: veerchinnathambi@gmail.com

S. Rajasekar
School of Physics, Bharathidasan Uuniversity, Thiruchirapalli-620 024, Tamilnadu, India.
e-mail: rajasekar@cnld.bdu.ac.in

Abstract: This paper invsetigates both analytically and numerically the effect of narrow band frequency modulated (NBFM) signal on horseshoe chaos in nonlinearly damped Duffing-vander Pol oscillator (DVP) system. Using the Melnikov analytical method, we obtain the threshold condition for the onset of horseshoe chaos. Threshold curves are drawn in various parameters spaces. We identify the regions of horseshoe chaos in various parameters spaces and bring out the effect of NBFM signal in DVP system. We illustrate that by varying the parameters f, g, p, one can suppress or enhance horseshoe chaos. We confirm the analytical results by the numerical tools such as computation of stable and unstable manifolds of saddle and threshold curves.

Keywords: Duffing-vander Pol oscillator, Nonlinear damping, NBFM signal, Horseshoe chaos, Melnikov method.

Manuscript accepted April 10, 2017.

1 Introduction

Over the past decades, a large number of analytical, numerical and experimental studies have been carried out on linearly damped nonlinear oscillator systems with an effort to understand the various features associated with the occurrence of chaotic behaviour [1-10]. Recently there have been attempts to study the effect of external periodic forces in certain nonlinearly damped nonlinear systems [11-25].

Horseshoe is the occurrence of transverse intersections of stable and unstable manifolds of a saddle fixed point in the Poincaré map and is a global phenomenon. In general, the existence of horseshoe does not imply that typical trajectories will be asymptotically chaotic. However the orbits created by the horseshoe mechanism display an extremely sensitive dependence on initial conditions and possibly exhibit either a chaotic transient before settling to stable orbits or strange attractor. Its appearance can be predicted analytically employing the Melnikov technique. Recently this method has been applied to certain nonlinear systems [5-11,13-19]. Nonlinearly damped Duffing-vander pol (DVP) oscillator under the influence of narrow band frequency modulated (NBFM) signal considered in the present paper is of the form

$$\ddot{x} + \gamma\, \dot{x}\, (1 - x^2)|\dot{x}|^{p-1} - \alpha^2 x + \beta x^3 = f(\cos\omega t - g \sin\Omega t \sin\omega t) \tag{1}$$

where $\gamma > 0$, $\alpha, \beta, \omega, \Omega$, p and f are constant parameters. DVP oscillator equation (Eq.1) serves as a basic model for self excited oscillations in Physics, Engineering, Electronics, Biology, Neurology and many other disciplines [1-8]. Recently the NBFM signal has been applied to certain nonlinear systems to investigate some nonlinear phenomena such as homoclinic bifurcations, stochastic and vibrational resonances etc. [26-29]. Our objective here is to explore the effect of NBFM signal on horseshoe chaos in Eq.(1) using both analytical and numerical techniques. In our present analysis, we use Melnikov analytical method to study the influence of NBFM signal on homoclinic orbits in Eq.(1).

2 Analytical results

In order to apply the Melnikov method to Eq.(1) we consider the system

$$\dot{x} = y \tag{2a}$$

$$\dot{y} = \alpha^2 x + \beta x^3 + \epsilon[\gamma\, (1 - x^2) y|y|^{p-1} + f(\cos\omega t - g \sin\Omega t \sin\omega t)] \tag{2b}$$

where ϵ is a small parameter. The unperturbed part of the system (Eq.2) with $\epsilon = 0$ has one saddle point $(x^*, y^*) = (0, 0)$ and two center type fixed points $(x^*, y^*) = (\pm\frac{\alpha}{\sqrt{\beta}}, 0)$. The two homoclinic orbits connecting the saddle to itself are given by

$$W^{\pm}(x_h(\tau), y_h(\tau)) = (\pm\alpha\sqrt{\frac{2}{\beta}}\, \mathrm{sech}\alpha\tau, \mp\alpha^2\sqrt{\frac{2}{\beta}}\, \mathrm{sech}\alpha\tau\, \tanh\alpha\tau), \qquad \tau = t - t_0 \tag{3}$$

The Melnikov theory [1, 2, 30] allows us to calculate the Melnikov function $M(t_0)$ for a classes of perturbed system for which homoclinic or heteroclinic orbit is known either analytically or numerically. $M(t_0)$ is proportional to the distance between the stable manifold

(W_s) and unstable manifold (W_u) of a saddle. When the stable and unstable manifolds are separated then the sign of $M(t_0)$ always remains same. $M(t_0)$ oscillates when W_s and W_u intersects transversely (horseshoe dynamics). The occurrence of transverse intersections implies the Poincaré map of the system has the so called *horseshoe chaos*.

From Eq.(2), the Melnikov function is worked out to be

$$M^{\pm}(t_0) = -\gamma \int_{-\infty}^{+\infty} |y_h|^{p+1} \left(1 - x_h^2\right)\ d\tau + f \int_{-\infty}^{+\infty} y_h \cos\omega(\tau + t_0)\ d\tau$$
$$-\frac{fg}{2} \int_{-\infty}^{+\infty} y_h \cos(\Omega - \omega)(\tau + t_0)\ d\tau + \frac{fg}{2} \int_{-\infty}^{+\infty} y_h \cos(\Omega + \omega)(\tau + t_0)\ d\tau \qquad (4)$$

Let $\omega_1 = (\Omega - \omega)$, $\omega_2 = (\Omega + \omega)$ and $G_1 = fg/2$

$\therefore$ the Eq.(4) becomes,

$$M^{\pm}(t_0) = -\gamma \int_{-\infty}^{+\infty} |y_h|^{p+1} \left(1 - x_h^2\right)\ d\tau + f \int_{-\infty}^{+\infty} y_h \cos\omega(\tau + t_0)\ d\tau$$
$$-G_1 \int_{-\infty}^{+\infty} y_h \cos\omega_1(\tau + t_0)\ d\tau + G_1 \int_{-\infty}^{+\infty} y_h \cos\omega_2(\tau + t_0)\ d\tau \qquad (5)$$
$$= \quad I_1 \quad + \quad I_2 \quad + \quad I_3 \quad + \quad I_4$$

(i) Evaluation of I_1

From Eq.(5), we have

$$I_1 \ = \ -\gamma \int_{-\infty}^{\infty} |y_h|^{p+1}\ (1 - x_h^2)\, d\tau$$

$$= \ -\gamma \int_{-\infty}^{\infty} |\, y_h\,|^{p+1}\ d\tau + \gamma \int_{-\infty}^{\infty} |\, y_h\,|^{p+1}\, x_h^2\, d\tau$$
$$= \qquad I_{11} \qquad + \qquad I_{12}$$

The evaluation of the integrals I_{11} and I_{12} gives the following results.

$$I_{11} = -\gamma(\alpha^2)^{p+\frac{1}{2}}\ \left(\frac{2}{\beta}\right)^{\frac{p+1}{2}}\ B\left[\frac{p+2}{2}, \frac{p+1}{2}\right]$$
$$I_{12} = \gamma(\alpha^2)^{p+\frac{3}{2}}\ \left(\frac{2}{\beta}\right)^{\frac{p+3}{2}}\ B\left[\frac{p+2}{2}, \frac{p+3}{2}\right]$$

Therefore,

$$I_1 = -\gamma(\alpha^2)^{p+\frac{1}{2}}\ \left(\frac{2}{\beta}\right)^{\frac{p+1}{2}}\ B\left[\frac{p+2}{2}, \frac{p+1}{2}\right] + \gamma(\alpha^2)^{p+\frac{3}{2}}\ \left(\frac{2}{\beta}\right)^{\frac{p+3}{2}}\ B\left[\frac{p+2}{2}, \frac{p+3}{2}\right] \qquad (6)$$

where $B(m,n)$ is the Euler Beta function which can be easily evaluated in terms of the Euler Gamma function. The relation connecting the Beta and Gamma function is

$$B(m,n) = \frac{\Gamma(m)\Gamma(n)}{\Gamma(m+n)} \tag{7}$$

where $\Gamma(m)$ denotes the Euler Gamma function

$$\Gamma(n) = \int_0^\infty e^{-x}x^{n-1}dx, \qquad n > 0 \tag{8}$$

(ii) Evaluation of I_2

From Eq.(5) we have,

$$\begin{aligned} I_2 &= f\int_{-\infty}^{\infty} y_h \cos\omega(\tau+t_0)\, d\tau \\ &= f\int_{-\infty}^{\infty} y_h(\cos\omega\tau\cos\omega t_0 - \sin\omega\tau\sin\omega t_0)\, d\tau \\ &= f\cos\omega t_0\int_{-\infty}^{\infty} y_h\cos\omega\tau d\tau - f\sin\omega t_0\int_{-\infty}^{\infty} y_h\sin\omega\tau d\tau \\ &= \qquad I_{21} \qquad + \qquad I_{22} \end{aligned}$$

After the evaluation of the integral I_{21}, the integral value of $I_{21} = 0$. The value of integral I_{22} is worked out to be

$$\begin{aligned} I_{22} &= \pm f\sin\omega t_0 \int_{-\infty}^{\infty} \alpha^2\sqrt{\frac{2}{\beta}}\,\text{sech}\alpha\tau\tanh\alpha\tau\sin\omega\tau d\tau \\ &= \pm\sqrt{\frac{2}{\beta}} f\pi\omega\ \text{sech}\ \left[\frac{\pi\omega}{2\alpha}\right]\sin\omega t_0 \end{aligned}$$

Therefore,

$$I_2 = \pm\sqrt{\frac{2}{\beta}} f\pi\omega\ \text{sech}\ \left[\frac{\pi\omega}{2\alpha}\right]\sin\omega t_0 \tag{9}$$

(iii) Evaluation of I_3

From Eq.(5) we have,

$$\begin{aligned} I_3 &= -G_1\int_{-\infty}^{\infty} y_h\cos\omega_1(\tau+t_0)\, d\tau \\ &= -G_1\int_{-\infty}^{\infty} y_h(\cos\omega_1\tau\cos\omega_1 t_0 - \sin\omega_1\tau\sin\omega_1 t_0)\, d\tau \\ &= -G_1\int_{-\infty}^{\infty} y_h\cos\omega_1\tau\cos\omega_1 t_0 d\tau + G_1\int_{-\infty}^{\infty} y_h\sin\omega_1\tau\sin\omega_1 t_0 d\tau \\ &= \qquad I_{31} \qquad + \qquad I_{32} \end{aligned}$$

The integral value of I_{31} is zero. The value of integral I_{32} is worked out to be

$$\begin{aligned} I_{32} &= G_1 \int_{-\infty}^{\infty} y_h \sin\omega_1\tau \sin\omega_1 t_0 d\tau \\ I_{32} &= -G_1 \sin\omega_1 t_0 \int_{-\infty}^{\infty} \alpha^2 \sqrt{\frac{2}{\beta}} \text{sech}\alpha\tau \tanh\alpha\tau \sin\omega_1\tau d\tau \\ &= \mp G_1 \sqrt{\frac{2}{\beta}} \pi\omega_1 \text{ sech}\left[\frac{\pi\omega_1}{2\alpha}\right] \sin\omega_1 t_0 \end{aligned}$$

Therefore,

$$I_3 = \mp G_1 \sqrt{\frac{2}{\beta}} \pi\omega_1 \text{ sech}\left[\frac{\pi\omega_1}{2\alpha}\right] \sin\omega_1 t_0 \tag{10}$$

(iv) Evaluation of I_4

Like the evaluation of I_3, the integral value of I_4 is obtained as

$$I_4 = \pm G_1 \sqrt{\frac{2}{\beta}} \pi\omega_2 \text{ sech}\left[\frac{\pi\omega_2}{2\alpha}\right] \sin\omega_2 t_0 \tag{11}$$

Therefore, Eq.(5) becomes

$$M^{\pm}(t_0) = A + B \ \pm \ C \ f \sin\omega t_0 \pm \ D \ G_1 \sin\omega_1 t_0 \pm \ E \ G_1 \sin\omega_2 t_0 \tag{12a}$$

where

$$A = -\gamma(\alpha^2)^{p+\frac{1}{2}} \ \left[\frac{2}{\beta}\right]^{\frac{p+1}{2}} \ B\left[\frac{p+2}{2}, \frac{p+1}{2}\right] \tag{12b}$$

$$B = \gamma(\alpha^2)^{p+\frac{3}{2}} \ \left[\frac{2}{\beta}\right]^{\frac{p+3}{2}} \ B\left[\frac{p+2}{2}, \frac{p+3}{2}\right] \tag{12c}$$

$$C = \sqrt{\frac{2}{\beta}} \ \pi\omega \text{ sech}\left[\frac{\pi\omega}{2\alpha}\right] \tag{12d}$$

$$D = -\sqrt{\frac{2}{\beta}} \ \pi(\Omega-\omega) \text{ sech}\left[\frac{\pi(\Omega-\omega)}{2\alpha}\right] \tag{12e}$$

$$E = \sqrt{\frac{2}{\beta}} \ \pi(\Omega+\omega) \text{ sech}\left[\frac{\pi(\Omega+\omega)}{2\alpha}\right] \tag{12f}$$

3 Numerical results

In this section we investigate the effect of NBFM signal on horseshoe chaos both analytically and numerically in the system (Eq.2) with the frequencies $\Omega = \omega$ and $\Omega \neq \omega$ cases respectively.

3.1 Effect of NBFM signal on horseshoe chaos for $G_1 = 0$ and $\Omega = \omega$

For $G_1 = 0$ and $\omega = \Omega$, the Eq.(12) becomes,

$$M^{\pm}(t_0) = A + B \ \pm \ C \ f \sin \omega t_0 \tag{13a}$$

The necessary condition for the occurrence of horseshoe chaos is

$$\mid f \mid \geq \mid f_m \mid = \gamma \left(\frac{2}{\beta}\right)^{\frac{p}{2}} \frac{(\alpha^2)^{p+\frac{1}{2}}}{\pi\Omega} \left\{ B\left[\frac{p+2}{2}, \frac{p+1}{2}\right] - \frac{2}{\beta}\alpha^2 \ B\left[\frac{p+2}{2}, \frac{p+1}{2}\right] \right\} \cosh\left(\frac{\pi\omega}{2\alpha}\right) \tag{13b}$$

The sufficient condition requires the existence of simple zeros of $M(t_0)$. Equality sign in Eq.13(b) corresponds to tangential intersections. In Fig.1, we plotted the threshold curve for horseshoe chaos in the $(f, \Omega(=\omega))$ plane for $\alpha = 1.0, \beta = 5.0, \gamma = 0.4$ and various p values.

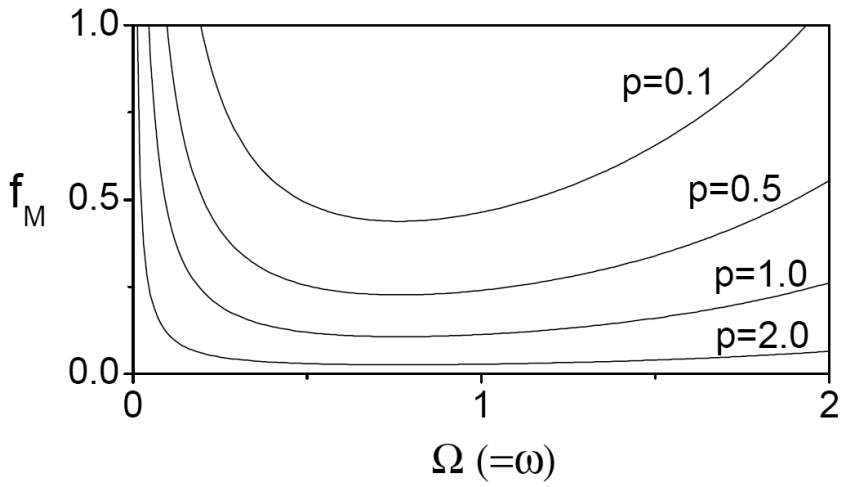

Figure 1: Melnikov threshold curves for horseshoe chaos in the $(f, \Omega(=\omega))$ plane for the system (Eq.2) driven by NBFM signal for various p values. The values of the other parameters in Eq.(2) are $\alpha = 1.0, \beta = 5.0, \gamma = 0.4$ and $g = 0.0$.

Below the curve, no transverse intersections of stable $(W_s^{\pm})$ and unstable $(W_u^{\pm})$ manifolds of the saddle occurs and above the curve, transverse intersections of stable $(W_s^{\pm})$ and unstable $(W_u^{\pm})$ occurs. Just above the Melnikov threshold curve, onset of cross-well chaos is expected. We have verified the analytical prediction by directly integrating the Eq.(2) using the fourth-order Runge-Kutta method. As an example, Fig.2 shows the part of the numerically computed stable and unstable orbits in the Poincaré map for $f = 0.1$ and $f = 0.3$ with $p = 0.5$ and $\Omega = \omega = 1$. The unstable manifolds are obtained by integrating the Eq.(1) in the forward time for a set of 900 initial conditions chosen around the perturbed saddle point. The stable manifolds are obtained by integrating the Eq.(1) in reverse time. For $f = 0.1$ the two orbits are well separated. In this parametric regime,

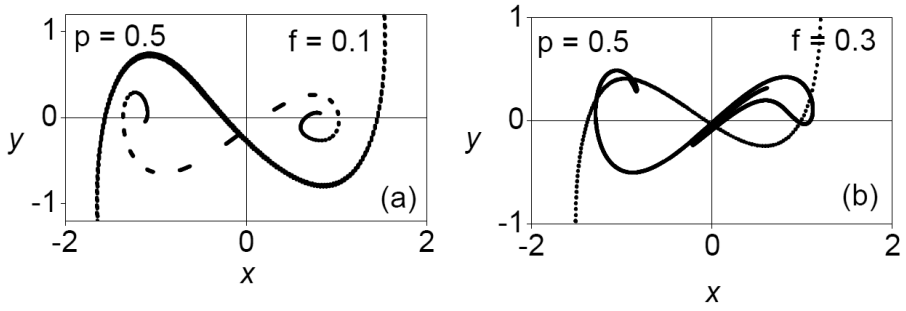

Figure 2: Numerically computed stable and unstable manifolds of the saddle fixed point of the system (Eq.2) driven by NBFM signal for (a) $f = 0.1$ and (b) $f = 0.3$ with $p = 0.5$. The values of the other parameters in Eq.(2) are $\alpha = 1.0, \beta = 5.0, \gamma = 0.4$ and $\Omega = \omega = 1.0$.

one may expect periodic behaviour. For $f = 0.3$ we can clearly notice transverse intersections of orbits at three places (Fig.2(b)). In this region, it is possible to have either asymptotic chaos or transient chaos followed by asymptotic periodic behaviour.

In order to know the nature of the attractors of the system near the horseshoe threshold value we have further numerically studied the Eq.(1) and the onset of cross-well chaos. Fig.3 shows the bifurcation and the corresponding maximal Lyapunov exponent diagrams for $p = 1.0$ and $p = 2.0$ with $g = 0.0$. From Fig.3, the onset of cross-well chaos are found to occur at $f = 0.12334$ for $p = 1.0$ and $f = 0.09674$ for $p = 2.0$. The analytically predicted Melnikov threshold values (f_M) for $p = 1.0$ and $p = 2.0$ are 0.125 and 0.09754. The analytical prediction is in good agreement with the actual numerical analysis of the system.

3.2 Effect of NBFM signal on horseshoe chaos for $G_1 \neq 0$ and $\Omega = \omega$

First we consider the effect of NBFM signal on horseshoe chaos in the system (Eq.2) by fixing the value of g and thereby varying f. For $\Omega = \omega$, we have D=0 in Eq.12(e) and the Melnikov function given by Eq.12(a) becomes,

$$M^{\pm}(t_0) = A + B \ \pm \ C\ f \sin \omega t_0 \pm \ E\ G_1 \sin 2\omega t_0 \tag{14a}$$

The necessary condition for the occurrence of horseshoe chaos is

$$f \ \geq \ f_M^{\pm} \ = (A \ + \ B \ \pm \ EG_1) \ / \ C \tag{14b}$$

(or)

$$f \ \leq \ f_M'^{\pm} \ = (-A \ - \ B \ \mp \ EG_1) \ / \ C \tag{14c}$$

where the superscripts sign $'+'$ and $'-'$ correspond to the homoclinic orbits W^+ and W^- respectively.

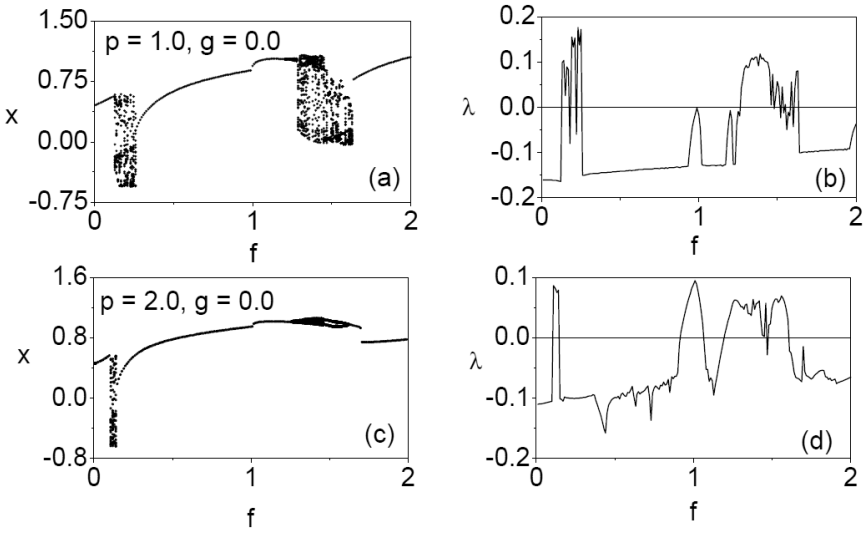

Figure 3: Bifurcation and the corresponding maximal Lyapunov exponent diagrams for the system (Eq.1) driven by NBFM signal for (a-b) $p = 1.0$ and (c-d) $p = 2.0$. The values of the other parameters in Eq.(1) are $\alpha = 1.0, \beta = 5.0, \gamma = 0.4, g = 0.0$ and $\Omega = \omega = 1.0$.

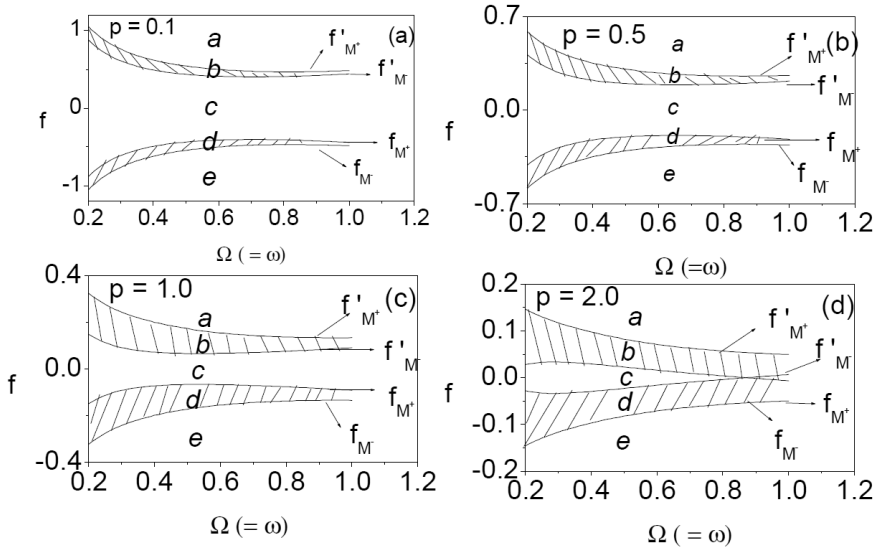

Figure 4: Melnikov threshold curves for horseshoe chaos in the $(f, \Omega(= \omega))$ plane for the system (Eq.2) driven by NBFM signal for four p values. The values of the other parameters in Eq.(2) are $\alpha = 1.0, \beta = 5.0, \gamma = 0.4$ and $g = 0.1$.

Figure 4 shows the threshold curves for the occurrence of horseshoe chaos in the $(f, \Omega(=\omega))$ plane for $\Omega = \omega$, $\alpha = 1.0, \beta = 5.0, \gamma = 0.4$, $g = 0.1$ and various p values. In the regions a and e both $M^+(t_0)$ and $M^-(t_0)$ change sign and the transverse intersections of stable and unstable parts of W^+ and W^- occur. $M^+(t_0)$ alone changes sign in the region b and hence transverse intersections of orbits of W^+ occur. In region c, no transverse intersections of both stable and unstable manifolds of saddle occur. In the region d, transverse intersections of (W_u^-) and unstable (W_s^-) alone take place. We verified this by direct simulation of the system (Eq.2). As an example, Fig.5 shows the part of stable and unstable orbits in the Poincaré map for four values of f chosen in the regions a, b, c and d with $\Omega = \omega = 1$, $g = 0.1$ and $p = 2.0$. Transverse intersections

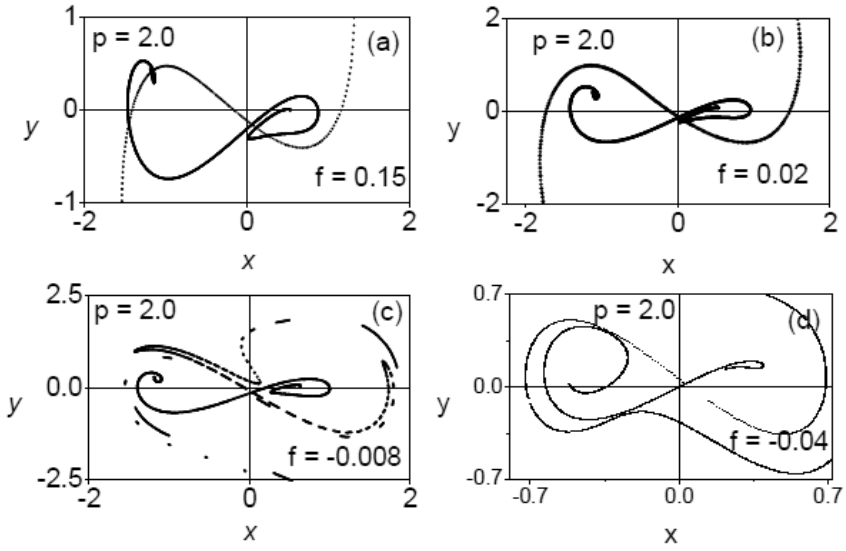

Figure 5: Numerically computed stable and unstable manifolds of the saddle fixed point of the system (Eq.2) driven by NBFM signal for four values of f chosen in the regions a, b, c and d with $p = 2.0$ and $g = 0.1$. The values of the other parameters in Eq.(2) are $\alpha = 1.0, \beta = 5.0, \gamma = 0.4$ and $\Omega = \omega = 1.0$.

of stable and unstable branches of both the homoclinic orbits $W_s^{\pm}$ and $W_u^{\pm}$ can be clearly seen in Fig.5(a) for $f = 0.15$ which falls in the region a. In Fig.5(b) we see the intersections of W_s^+ and W_u^+ orbits alone at one place for $f = 0.02$ (region b) while for $f = -0.008$ (region c) no transverse intersection of orbits occur. This is shown in Fig.5(c). For $f = -0.04$ (Fig.5(d)) which corresponds to the region d, branches W_s^- and W_u^- alone intersect.

Next we analyze the effect of NBFM signal on horseshoe chaos for a fixed value of f and thereby varying g. The necessary condition on g for $M(t_0)$ to change sign is

$$G_1 \geq G_{1M}^{\pm} = (A + B \pm Cf) / E \tag{15a}$$

$$G_1 \leq G_{1M}^{\prime\pm} = (-A - B \mp Cf) / E \tag{15b}$$

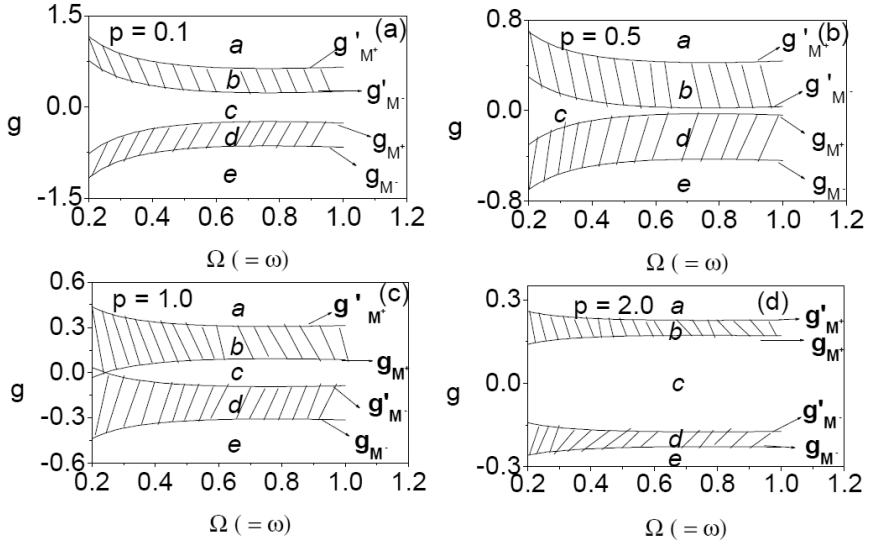

Figure 6: Melnikov threshold curves for horseshoe chaos in the $(g, \Omega(=\omega))$ plane for the system (Eq.2) driven by NBFM signal for four p values. The values of the other parameters in Eq.(2) are $\alpha = 1.0, \beta = 5.0, \gamma = 0.4$, and $f = 0.2$.

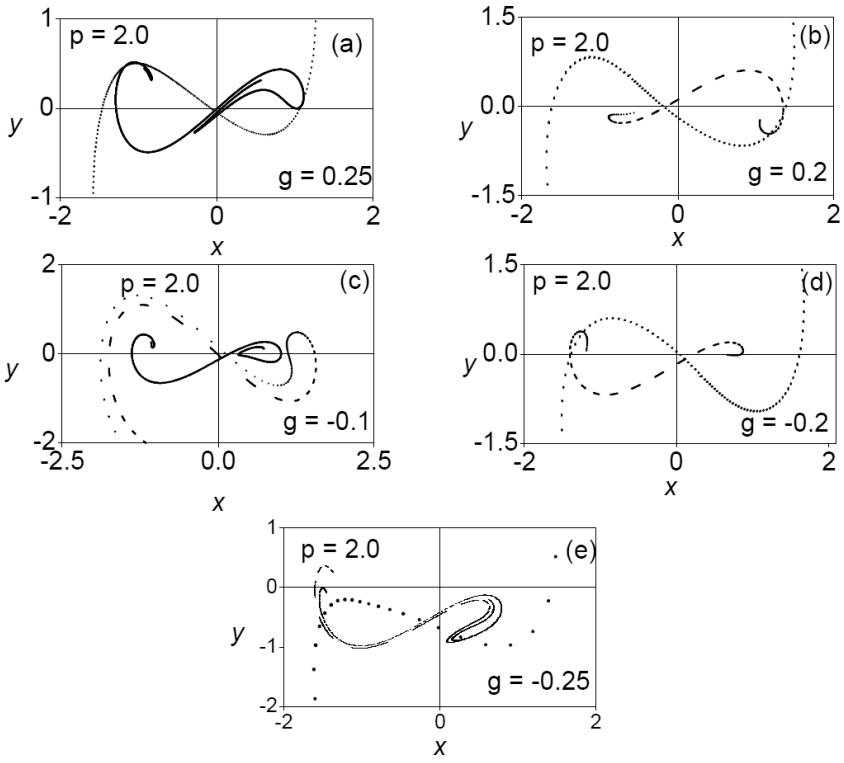

Figure 7: Numerically computed stable and unstable manifolds of the saddle fixed point of the system (Eq.2) driven by NBFM signal for five values of g with $p = 2.0$. The values of the other parameters in Eq.(2) are $\alpha = 1.0, \beta = 5.0, \gamma = 0.4$ $f = 0.2$ and $\Omega = \omega = 1.0$.

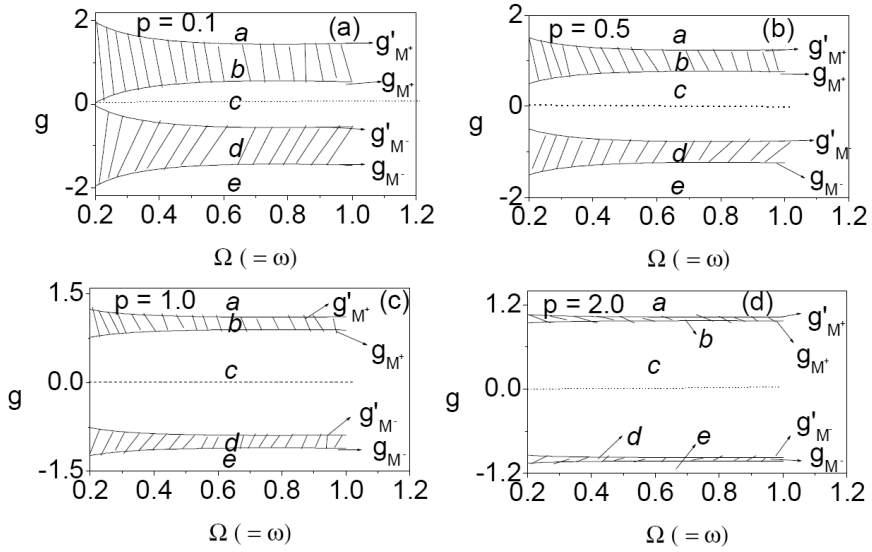

Figure 8: Melnikov threshold curves for horseshoe chaos in the $(g, \Omega(=\omega))$ plane for the system (Eq.2) driven by NBFM signal for four p values. The values of the other parameters in Eq.(2) are $\alpha = 1.0, \beta = 5.0, \gamma = 0.4$ and $f = 1.0$.

Figure 6 shows the Melnikov threshold curves for horseshoe chaos in the $(g, \Omega(=\omega))$ plane for $f = 0.2$ with four values of p. For $p = 2.0$, we have verified the above analytical results by direct simulation of the system (Eq.2). Figure 7 shows the part of stable and unstable orbits in the Poincaré map for five values of g chosen in the regions a, b, c, d and e with $\Omega = \omega = 1$ and $f = 0.2$. Then we fixed $f = 1.0$ above the threshold values for all the values of p with $g = 0.0$ and studied the effect of modulating term by varying g. Figure 8 shows the Melnikov threshold curves for $f = 1.0$. When $f = 1.0$ and $g = 0.0$ transverse intersections of stable and unstable manifolds of saddle occur for a range of ω (see Fig.1). This is represented by the straight line in Fig.8. When g is switched on even for small values of g, transverse intersections suddenly disappear. That is horseshoe chaos is suppressed. This occurs for a range of values of g.

3.3 Effect of NBFM signal on horseshoe chaos for $G_1 \neq 0$ and $\Omega \neq \omega$

In the previous section we studied the effect of NBFM signal on horseshoe chaos for the case of $\Omega = \omega$. In this section, we consider the case $\Omega \neq \omega$. For this case, we cannot write the necessary condition for the occurrence of horseshoe chaos similar to Eq.(14) or (15). However the occurrence of horseshoe chaos can be studied numerically measuring the time τ_M elapsed between the successive transverse intersection. τ_M can be determined from Eq.(12). Figure 9 shows the variation of $1/\tau_M^{\pm}$ versus f for $\omega = 1.0$, $\Omega = \sqrt{2}$, $\alpha = 1.0, \beta = 5.0, \gamma = 0.4$, $g = 0.1$ and four values of p. Continuous curves represent the inverse of first intersection time $1/\tau_M^{\pm}$ of stable and unstable branches of homoclinic

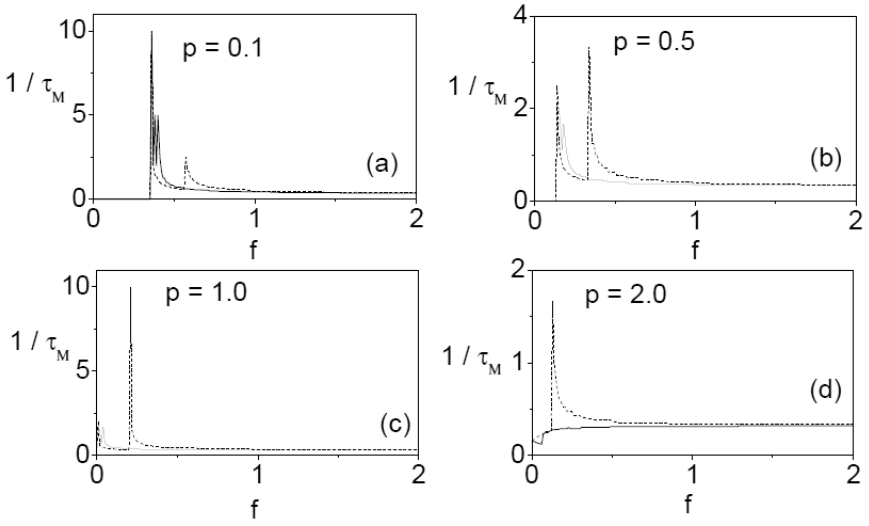

Figure 9: Variation of $1/\tau_M^{\pm}$ versus f for $g = 0.1$, $\omega = 1.0$, $\Omega = \sqrt{2}$ and four values of p. The values of the other parameters in Eq.(2) are $\alpha = 1.0, \beta = 5.0$ and $\gamma = 0.4$.

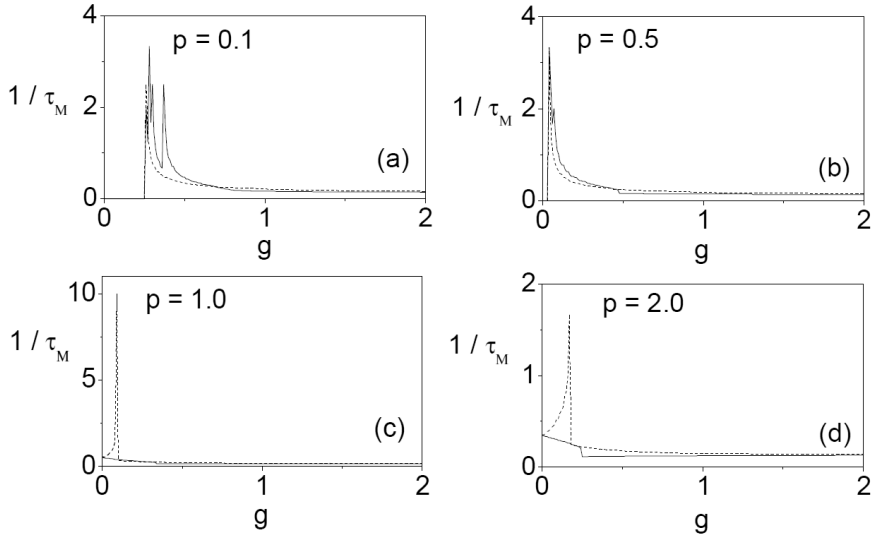

Figure 10: Variation of $1/\tau_M^{\pm}$ versus g for $f = 0.2$, $\omega = 1.0$, $\Omega = \sqrt{2}$ and four values of p. The values of the other parameters in Eq.(2) are $\alpha = 1.0, \beta = 5.0$ and $\gamma = 0.4$.

orbits W^+. Dashed curves correspond to the orbits of W^-. Horseshoe chaos does not occur when $1/\tau_M^{\pm}$ is zero and it occurs in the region when $1/\tau_M^{\pm} > 0$. In Fig.9, when the value of g is fixed at 0.1, $1/\tau_M^{\pm}$ are zero for $0 < f < 0.35792$ for $p = 0.1$ (Fig.9(a)), $0 < f < 0.13785$ for $p = 0.5$ (Fig.9(b)), $0 < f < 0.01935$ for $p = 1.0$ (Fig.9(c)) and hence no horseshoe chaos occurs in this interval of f. For the other values of f, $1/\tau_M^{\pm}$ are nonzero, that is, horseshoe chaos occurs. Figure 10 shows the plot of $1/\tau_M^{\pm}$ against g for $\alpha = 1.0, \beta = 5.0, \gamma = 0.4, f = 0.2, \omega = 1.0$ and $\Omega = \sqrt{2}$. In Fig.10, $1/\tau_M^{\pm}$ are zero for $0 < g < 0.25227$ for $p = 0.1$ (Fig.10(a)) and $0 < g < 0.03458$ for $p = 0.5$ (Fig.10(b)). For other values of g, $1/\tau_M^{\pm}$ are nonzero.

4 Conclusion

The study of the effect of NBFM signal on horseshoe chaos is carried out in nonlinearly damped DVP system (Eq.2). Both analytically and numerically we studied the effect of NBFM signal on horseshoe chaos in DVP system (Eq.2). Applying Melnikov analytical method we obtained the threshold condition for onset of horseshoe chaos, that is, transverse intersection of stable and unstable branches of homoclinic orbits. Threshold curves are drawn on different parameters spaces. We demonstrated the effect of the parameters f, g, Ω and p on the dynamics of the system (Eq.2).

When the damping exponent (p) increases from small values, the threshold value decreases for onset of horseshoe chaos. The introduction of nonlinear damping term affects the various nonlinear behaviours such as period doubling route to chaos, crises, threshold values for the horseshoe chaos etc. For typical parametric values, we have shown the suppression and enhancement of horseshoe chaos due to the effect of nonlinear damping and NBFM signal. Analytical prediction of horseshoe chaos is found to be in good agreement with numerical simulation of the system (Eq.2). In the present work, we studied the effect of NBFM signal on horseshoe chaos in system (Eq.2) with symmetric potential. It is important to study the effect of nonlinear damping and NBFM signal with three different asymmetric potentials . These will be investigated in future.

References

[1] J. Guckenheimer and P. Holmes, The Nonlinear Oscillations, Dynamical Systems and Bifurcations of Vector Fields, *(Springer, New York, 1983).*

[2] S. Wiggins, Introduction to Applied Nonlinear Dynamical Systems and Chaos, *(Springer, New York, 1990).*

[3] E. Ott, Chaos in Dynamical Systems, *(Cambridge University Press, New York, 1993).*

[4] M. Lakshmanan and S. Rajasekar, Nonlinear Dynamics: Integrability, Chaos and Patterns, *(Springer, Berlin, 2003).*

[5] S. Rajasekar, Controlling of Chaos by Weak Periodic Perturbations in DVP Oscillator, *Pramana J. of Physics*, 41, 295-309, 1993.

[6] Z. Zing, Z. Yang and T. Jiang, Complex Dynamics in DVP equation, *Chaos, Solitons and Fractals*, 27, 722-747, 2006.

[7] L. Ravisankar, V. Ravichandran and V. Chinnathambi, Prediction of Horseshoe Chaos in Duffing-vander Pol Oscillator Driven by Different Periodic Forces, *Int. J. of Eng. and Sci.*, 1(5), 17-25, 2012.

[8] S. Rajasekar, S. Parthasarathy and M. Lakshmanan, Prediction of Horseshoe Chaos in BVP and DVP Oscillators, *Chaos, Solitons and Fractals*, 2(3), 271-280, 1992.

[9] V. Ravichandran, V. Chinnathambi, S. Rajasekar and C.H. Lai, Effect of the Shape of Periodic Forces on Horseshoe Chaos in Duffing Oscillator, *arXiv: 0808 0406V1 [nlin.CD]*, 4 Aug 2008.

[10] V. Ravichandran, V. Chinnathambi and S. Rajasekar, Homoclinic Bifurcation and Chaos in Duffing Oscillator Driven by an Amplitude Modulated Force, *Physica A*, 376, 223-236, 2007.

[11] J.P. Baltanas, J.L. Trueba and M.A.F. Sanjuan, Energy Dissipation in a Nonlinearly Damped Duffing Oscillators, *Physica D*, 159, 22-34, 2001.

[12] S.J. Elliot, M. Ghandchi Tehrani and R.L. Langley, Nonlinear Damping and Quasi-Linear Modelling, *Phil. Frans. R. Soc. A*, 373, 20140402. http:// dx.doi.org/10.1098/rsta.2014.0402 -30pp, 2015.

[13] Z.M. Ge and C.Y. Ou, Chaos in a Fractional Order Modified Duffing System, *Chaos, Solitons and Fractals*, 14, 262-291, 2007.

[14] J.L. Trueba, J. Rams and M.A.F Sanjuan, Analytical Estimates of the Effect of Nonlinear Damping in Some Nonlinear Oscillators, *Int. J. Bifur. and Chaos*, 10(9), 2257-2267, 2000.

[15] M. Borowice, G. Litak and A. Syta, Vibration of the Duffing Oscillator; Effect of Fractional Damping, *Shock and Vibration*, 14, 29-36, 2007.

[16] M.A.F. Sanjuan, The Effect of Nonlinear Damping on the Universal Escape Oscillator, *Int. J. of Bifur. and Chaos*, 9, 735-744, 1999.

[17] G. Litak, M. Borowiee and A. Syta, Vibration of Generalized Double-well DVP oscillator, *arXiv:nlin/0610052v1 [nlin.CD]*, 20 Oct 2006.

[18] M.V. Sethumeenakshi, S. Athisayanathan, V. Chinnathambi and S. Rajasekar, *Effect of Fractional Damping in Double-Well DVP Oscillator Driven by Different Sinusoidal Periodic Forces* , (Submitted for Publication, 2016).

[19] M.V. Sethumeenakshi, S. Athisayanathan, V. Chinnathambi and S. Rajasekar, Effect of Fractional Damping in Double-Well DVP oscillator Driven by Different Nonsinusoidal Periodic Forces, (Submitted for Publication, 2016).

[20] J. Padovan and J.T. Sawicki, Nonlinear Vibration of Fractional Damped Systems, *Nonlinear Dynamics*, 16, 321-336, 1998.

[21] R.E. Mickens, K.O. Oyedeji and S.A. Rucker, Analysis of the Simple Harmonic Oscillator with Fractional Damping, *J. Sound and Vib.*, 268, 839-842, 2003.

[22] L.J. Shen, H.K. Chen, J.H. Chen and L.M. Tam, Chaotic Dynamics of the Fractionally Damped Duffing Equation, *Chaos, Solitons and Fractals*, 31, 1203-1212, 2007.

[23] L. Cveticanin, Oscillator With Strong Quadratic Damping Force, *Publications de L'institute of Mathematique, Nouville Serie, Tome*, 85, 119-130, 2009.

[24] B. Ravindra and A.K. Mallik, Stability Analysis of a Nonlinearly Damped Duffing Oscillator, *J. Sound. Vib.*, 171, 708-716, 1994.

[25] B. Ravindra and A.K. Mallik, Role of Nonlinear Dissipation in Soft Duffing Oscillators, *Phys. Rev. E*, 49, 4950-4954, 1994.

[26] L. Ravisankar, V. Ravichandran, V. Chinnathambi and S. Rajasekar, Effect of Narrow Band Frequency Modulated Force on Horseshoe Chaos in Duffing-vander Pol Oscillator, *Int. J. of Sci. and Eng. Res.*, 48, 1155-1162, 2013.

[27] L. Ravisankar, V. Ravichandran, V. Chinnathambi and S. Rajasekar, Horseshoe Dynamics in Asymmetric Duffing-vander Pol Oscillator Driven by Narrow Band Frequency Modulated Force, *Chinese J. of Physics*, 52(3), 1026-1043, 2014.

[28] Y.C. Lai, Z. Liu, A. Nachman and L. Zhen, Suppression of Jamming in Excitable System by Aperiodic Stochastic Resonance, *Int. J. of. Bifur. and Chaos*, 14, 3519-3539, 2000.

[29] S. Guruparan, B. Ravindran Durai Nayagam, V. Ravichandran, V. Chinnathambi and S. Rajasekar, Vibrational Resonance in the Classical Morse Oscillator Driven by NBFM and WBFM Signals, *Journal of Pure Applied Chemical Research*, 5(3), 131-141, (2016).

[30] F.C Moon and G.X. Li, Fractal Basin Boundaries and Homoclinic Orbits for Periodic Motions in a Two-Well Potential, *Phys. Rev. Lett.*, 55, 1439-1442, 1985.